Chemical Science

ROYAL SOCIETY OF CHEMISTRY

EDGE ARTICLE

View Article Online
View Journal | View Issue

Cite this: *Chem. Sci.*, 2021, **12**, 15263

All publication charges for this article have been paid for by the Royal Society of Chemistry

Ternary complexes of chiral disulfonimides in transfer-hydrogenation of imines: the relevance of late intermediates in ion pair catalysis†

Matej Žabka and Ruth M. Gschwind *

In ion pairing catalysis, the structures of late intermediates and transition states are key to understanding and further development of the field. Typically, a plethora of transition states is explored computationally. However, especially for ion pairs the access to energetics *via* computational chemistry is difficult and experimental data is rare. Here, we present for the first time extensive NMR spectroscopic insights about the ternary complex of a catalyst, substrate, and reagent in ion pair catalysis exemplified by chiral Brønsted acid-catalyzed transfer hydrogenation. Quantum chemistry calculations were validated by a large amount of NMR data for the structural and energetic assessment of binary and ternary complexes. In the ternary complexes, the expected catalyst/imine H-bond switches to an unexpected O–H–N structure, not yet observed in the multiple hydrogen-bond donor–acceptor situation such as disulfonimides (DSIs). This arrangement facilitates the hydride transfer from the Hantzsch ester in the transition states. In these reactions with very high isomerization barriers preventing fast pre-equilibration, the reaction barriers from the ternary complex to the transition states determine the enantioselectivity, which deviates from the relative transition state energies. Overall, the weak hydrogen bonding, the hydrogen bond switching and the special geometrical adaptation of substrates in disulfonimide catalyst complexes explain the robustness towards more challenging substrates and show that DSIs have the potential to combine high flexibility and high stereoselectivity.

Received 8th July 2021
Accepted 22nd October 2021

DOI: 10.1039/d1sc03724b

rsc.li/chemical-science

Introduction

The detection and identification of reaction intermediates in asymmetric catalysis still poses considerable challenges to the experimental setup as well as to the computational elucidation of possible structures. This quest is even more difficult in the area of noncovalent organocatalysis, where well-defined hydrogen-bonded or ion-pair intermediates are rather scarcely detected and offsets between experimental and computational populations limit the explanatory power of calculations.[1,2] One of the central model systems for mechanistic investigations in ion pair catalysis is the enantioselective Brønsted acid-catalysed transfer-hydrogenation of imines.[3–5] This reaction represents a general and mild route to the synthesis of chiral amines, which are valuable structural units found in many bioactive compounds.[6–8] The early intermediates in the corresponding catalytic cycle, the binary complexes of the catalysts and imines as well as their dimers, have already been experimentally detected.[9,10] Even the dynamic behaviour of these species could be followed by NMR.[11] However, later intermediates and transition states were proposed for the purely organocatalytic chiral phosphoric acid (CPA)-catalysed reaction only by theoretical calculations.[12–16] The computed active transition states suggested that the reaction proceeds *via* the bifunctional binding of both the substrate and the reagent by the catalyst.[17–19]

So far mechanistic studies have focused mainly on popular catalysts employed for the transfer-hydrogenation such as chiral phosphoric acids *e.g.* TRIP **1**, and the more acidic disulfonimides **2** (see Fig. 1A).[20–26] These widely used catalysts benefit from the axially chiral BINOL backbone, whose 3,3′-substituents can be fine-tuned for the desired reactivity and selectivity.[14] The role of the catalysts in the catalytic cycle was studied using experimental and computational methods. The first step of the proposed catalytic cycle is the formation of an *E*-imine binary complex. Given sufficient thermal energy, the catalyst is capable of isomerizing the *E*-complex into a *Z*-imine complex, which are in slow exchange at 180 K, as shown by NMR studies by our group (Fig. 1B).[27]

We have also reported that for the complexes of CPAs, a strong, charge-assisted hydrogen bond is formed, as evidenced by the detection of $^{1}J_{NH}$ and $^{3}J_{PH}$ scalar couplings across the H-bond, with additional noncovalent CH–π and π–π interactions. This evidence is supported by the correlation of hydrogen bond strength and NMR parameters such as ^{1}H and

Institute of Organic Chemistry, University of Regensburg, D-93053 Regensburg, Germany. E-mail: ruth.gschwind@chemie.uni-regensburg.de

† Electronic supplementary information (ESI) available. See DOI: 10.1039/d1sc03724b

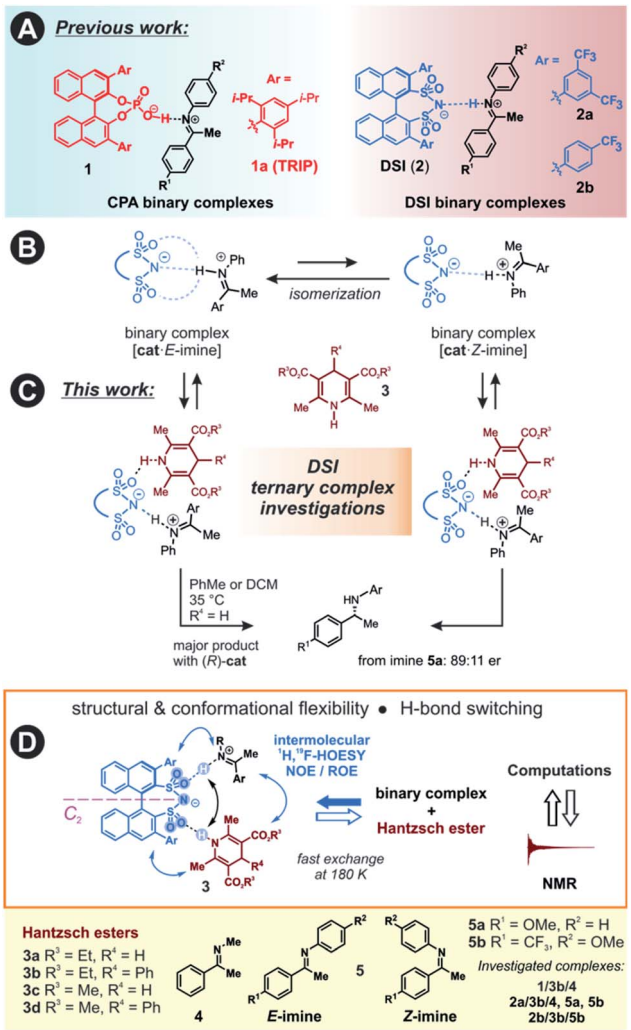

Fig. 1 (A) Previously, binary complexes of CPA (**1**) with a strong, charge-assisted H-bond, and DSI (**2**) catalysts with imines **4**–**5** having a weak H-bond were investigated by NMR in detail. (B) Binary complexes of catalysts and imines are in *E*/*Z*-equilibrium. (C) In this work, we present the detection and analysis of ternary complexes of catalysts, imines and Hantzsch ester. (D) Intermolecular ^{1}H,^{1}H-NOESY/ROESY and ^{1}H,^{19}F-HOESY experiments showed the presence of a ternary complex with soluble Hantzsch esters **3**. The ternary complex is in fast exchange with the binary complex even at 180 K, and the Overhauser effect from the ternary complex can be detected.

^{15}N chemical shifts in the Steiner–Limbach plot.[9] In contrast, chiral DSIs form rather weak hydrogen bonds with imines and the complexes have more ion-pair character, allowing some additional structural flexibility.[28,29]

The reducing agent then approaches the binary complex. The reaction utilizes a sacrificial hydrogen donor, such as Hantzsch ester, to transfer a hydride ion to the LUMO-activated imine.[30–32]

The chiral catalyst in the complex is proposed to establish a new hydrogen bond to the reducing agent due to its bifunctional nature, thus enhancing the thermodynamic driving force for the hydride transfer (see Fig. 1C for principal arrangements in case of DSI).[33] An analogous activation has been suggested in a bifunctional thiourea-catalysed transfer hydrogenation.[34] With such dual activation offering an opportunity for efficient chirality transfer, a ternary complex is formed and chiral information is transmitted. The catalyst is then liberated from the complex and a proton transfer from the formed pyridinium ion ensures the regeneration of the catalyst, which can enter a new catalytic cycle. Based on extensive experimental evidence, the *E*/*Z*-isomerization and the ternary complex formation have been proposed to be the potential rate-determining steps in the cycle.[35] As a result, the availability and detectability of the ternary complex in the reaction mixture is extremely limited.

Moreover, the bifunctional binding mode is a crucial factor for the reactivity, often overriding the acidity of the catalyst towards faster reaction rates. This has been demonstrated by comparing the reaction rates of DSI or its simple analogues compared to HCl as the monofunctional catalyst.[36] Moreover, we have shown that a very acidic bis(sulfonic) acid catalyst gave the slowest reaction most likely due to the intramolecular H-bond stabilization of the resulting monosulfonate.[28]

However, the bifunctional binding of the substrate and reducing agent to the classical CPAs has not been experimentally disclosed so far. This topic is even more pressing with the far more complex situations in multiple H-bond acceptors present in the recently developed, highly-acidic ion pair catalysts. To the best of our knowledge, NMR based experiments – without extensive NOE map and the geometries proposed only by semi-empirical methods – were obtained exclusively for an organometallic Ir-catalyst and imine.[37] In addition, many computational methods reproduce geometries of ion pair complexes reliably. However, the relative experimental populations of the binary complexes could not be reproduced by computations without large deviations so far, which raises questions about the correct evaluation of transition states.

Here, we present the first experimental proof for H-bonded ternary complexes of chiral disulfonimides (DSI) with imines and Hantzsch ester based on detailed NOE analysis, H-bond detection, relaxation and diffusion studies, and chemical shift perturbation analysis. The combination of these experimental data allowed us to select a computational method, which reproduced the experimental populations of the complexes. The NMR and computational analyses revealed the switching of weak H-bonds in multi-acceptor situations from the expected N–H–N pattern to an O–H–N binding in ternary complexes (see Fig. 1D). This unexpected feature has not yet been considered in the design stage of catalyst development so far. Moreover, the data showed that the inclusion of ground states is indispensable when assessing transition states of reactions where isomerization of intermediates is a slow process.

Results and discussion

Model systems and experimental setup

Two catalysts, (*R*)-TRIP (**1**) and (*R*)-DSI (**2**) were tested as model systems. Our previous efforts in establishing the ternary complex of TRIP (**1**) have been hampered by the extremely low solubility of the Hantzsch ester **3a**.[35] Furthermore, the inevitable formation of reaction products during the sample

preparation complicated the analysis of 1D ^{1}H NMR spectra at low temperatures. To solve both issues, we employed ester **3b** which contains an additional phenyl group, distant from the potential binding site, and is also fully soluble at 180 K (see Fig. 1D). As imine we chose the small-sized *N*-Me imine **4** to minimize the impact of the steric interactions, since previous studies with larger imines were unfruitful.[35]

Only for DSIs **2**, homogenous solutions at 180 K are formed, relatively sharp peaks are present and even intermolecular NOEs/HOEs are detected between signals of iminium, catalysts **2** and Hantzsch ester **3b**. Similar intermolecular NOEs/HOEs hinting at ternary complex formation were observed using *N*-aryl imines [^{15}N]-**5a** and **5b** (Fig. 1D). Generally, the binary complex of DSI and imine is in fast exchange with the ternary complex and only average signals are observed (*e.g.*, $\delta_{\text{H-bond}}$ (*E*) 14.53/(*Z*) 15.06 ppm in **2b**/**3b**/**5b**, signals are split by $^{1}J_{\text{NH}}$ in the ^{15}N-labelled imines and Hantzsch ester) (for further discussion and exclusion of other possibilities see ESI Chapter 6.2†).

The NMR spectra generally show the major *E*- and minor *Z*-iminium ions, with the hydrogen bond in slow mutual exchange. No free imines are detected in the samples, because the imines are protonated by the acidic catalysts. There is one set of signals for the Hantzsch ester with split 2,6-dimethyl group signal; and only one set of signals for the catalyst, accompanied by averaging of the signals of its two naphthyl groups (Fig. 1D). This averaging suggests a fast equilibrium with the binary complex coupled to a fast rotation around the catalyst's C_2-axis. Interestingly, the rotation of the 3,3′-substituents is hindered in DSI complexes. For example, two distinct ^{19}F signals are present for the catalyst **2a**, and two ^{1}H AB systems for catalyst **2b**. Thus, we could confirm the presence of the ternary complex with DSI catalysts by NMR and exclude the possibility of the Overhauser effects stemming from separate Hantzsch ester complexes.

Hantzsch ester binding and *Z*-imine complex

To address the binding site and the binding constant, the chemical shift perturbation upon the binding of Hantzsch ester to the binary complex was investigated. Therefore, **3b** (0.5–15 eq.) was sequentially added to the binary complex **2a**/**5a** (20 mM) and ^{1}H and ^{1}H,^{13}C-HSQC spectra were recorded at 180 K to allow for chemical shift mapping (Fig. 2A). In general, the signals of the *Z*-complex showed significantly larger chemical shift perturbations than the *E*-complex (see 1D spectrum in Fig. 2A). For the *Z*-complex the iminium ^{15}NH was shifted followed by protons *Z*-1/*Z*-2 (see Fig. 2A and ESI Chapter 8†). Fitting these data for two distinct sites (*Z*-NH and *Z*-2 CH) revealed a binding constant K_a = ~22, indicating a weak binding of the Hantzsch ester to the binary *Z*-complex. For the *E*-complex, only the iminium NH and the methoxy group showed small chemical shift differences (see *E*-NH and *E*-1 in Fig. 2A and in the ^{1}H,^{13}C-HSQC spectrum ESI Chapter 8†). The nearly linear change suggests a much weaker binding of the *E*-complex.

The population of *Z*-complexes was then doubled from 15% to 31% by photoisomerisation (back isomerization is stopped at

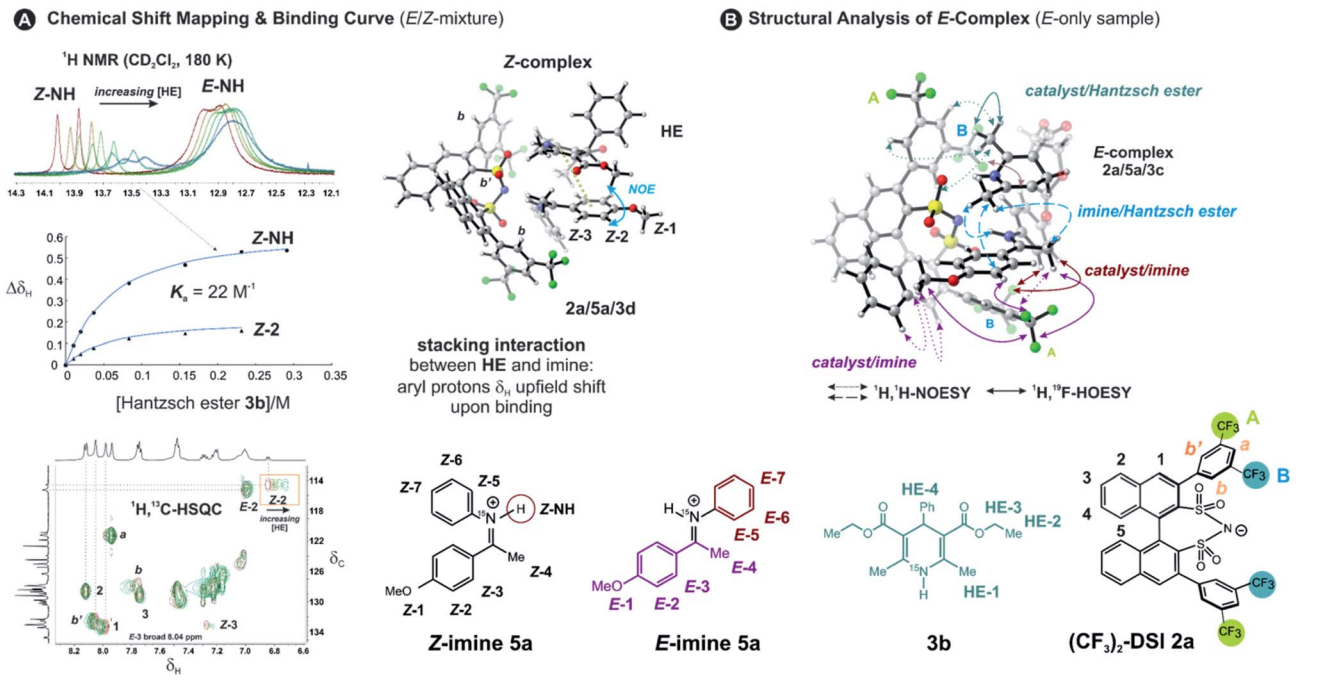

Fig. 2 Chemical shift mapping and NOE/HOE analysis proves bifunctional binding in the ternary complex: (A) stronger binding of *Z*-imine from chemical shift mapping: NMR titration of $(CF_3)_2$-DSI **2a**/**5a** *E*/*Z* mixture (20 mM) with 0–15 eq. Hantzsch ester **3b**, followed by ^{1}H NMR and ^{1}H,^{13}C-HSQC spectra in CD_2Cl_2 at 180 K (NH signals split into doublets by $^{1}J_{\text{NH}}$ due to the iminium ^{15}N nucleus). Fitting of the $\Delta\delta_H$ (*Z*-NH and *Z*-2) gave a binding constant K_a = 22 M^{-1} for *Z*-**5a**. The plausible calculated structure **2a**/**5a**/**3d** (TPSS-D3(BJ)/def2-SVP/SMD(CH_2Cl_2)) shows the NOE contact and explains the most pronounced chemical shift differences for *Z*-2/*Z*-3 resonances upon binding. (B) A plausible calculated structure of ternary of *E*-complex **2a**/**5a** with Hantzsch ester **3c** with key NOE and HOE contacts shown.

180 K). One intermolecular NOE contact between *Z*-2 of the iminium and the Hantzsch ester could be detected (see structure in Fig. 2A), which fits perfectly to the chemical shift perturbation and the calculated bifunctional structure of the ternary *Z*-complex. Thus, the chemical shift perturbation study in combination with the NOE detected corroborates the bifunctional binding of both imine and Hantzsch ester in the ternary complex for the first time spectroscopically.

NMR structural investigations of *E*-ternary complexes

Next, structural insights about the *E*-ternary complex were gained. Here, we prepared exclusively *E*-iminium complexes to reduce chemical shift overlap and to compensate for the smaller binding constant by increased concentrations. These samples were prepared by mixing solutions of imines and catalysts/Hantzsch ester mixtures at −80 °C to avoid any acid-promoted, thermal *E*/*Z* isomerization. Despite the low binding constant, 2D ^{1}H,^{1}H-NOESY spectra (CD_2Cl_2, 180 K) with short mixing times (50–100 ms) showed unexpectedly many intermolecular NOEs and (and HOEs) especially between the Hantzsch ester **3b**, the catalyst **2a** and the *E*-imine **5a** signals (see Fig. 2B) proving again the existence of a ternary complex. To exclude potential spin diffusion artifacts,[38,39] we collected 2D ^{1}H,^{1}H-ROESY data, which confirmed the observed contacts as genuine. A relevant population of a ternary complex is indicated by the significant intensity of the ROESY and ^{1}H,^{19}F-HOESY crosspeaks between the catalyst and the Hantzsch ester, as well as between the Hantzsch ester and the imine. The NOE/HOE signals to the Hantzsch ester are thus decisive about the ternary structure (Fig. 2B).

To get further insight about this potential conformational flexibility within the ternary complex, we utilized imine **5b** with an additional CF_3 group as a spectroscopic sensor together with catalyst CF_3-DSI **2b**. The three CF_3 groups allowed us to observe ^{1}H,^{19}F-HOESY signals between both the catalyst and Hantzsch ester as well as imine and Hantzsch ester (Fig. 3A and B), originating from the transiently formed ternary complex. Additionally, DOSY experiment at 180 K showed the three components – Hantzsch ester, imine, and the catalyst – diffuse together, corroborating the formation of a supramolecular complex (see ESI Chapter 11†). The estimated molecular mass matches the mass of the ternary complex. Typical NOE contacts were found for the two different conformations of the previously established *E*-imine binary complex (see Fig. 3C): *E*I (E_N/E_OI) which has the imine aryl next to the naphthyl group of the catalyst; and *E*II, which has the *N*-aryl ring close to the catalyst naphthyl ring. Since NOE contacts between the catalyst and the imine observed in the ternary mixtures originate from both binary and ternary complexes, we used only the contacts of the Hantzsch ester to the catalyst or the imine to reveal the ternary complex conformations (see ESI Chapter 7†). However, it seems that a new conformation, not populated in binary complexes is adopted which can accommodate all the observed NOE/HOE contacts. This anticipated structure could have an intermediate position of the imine between *E*I and *E*II structures, as was already observed for CPAs, namely in the CPA/imine dimeric

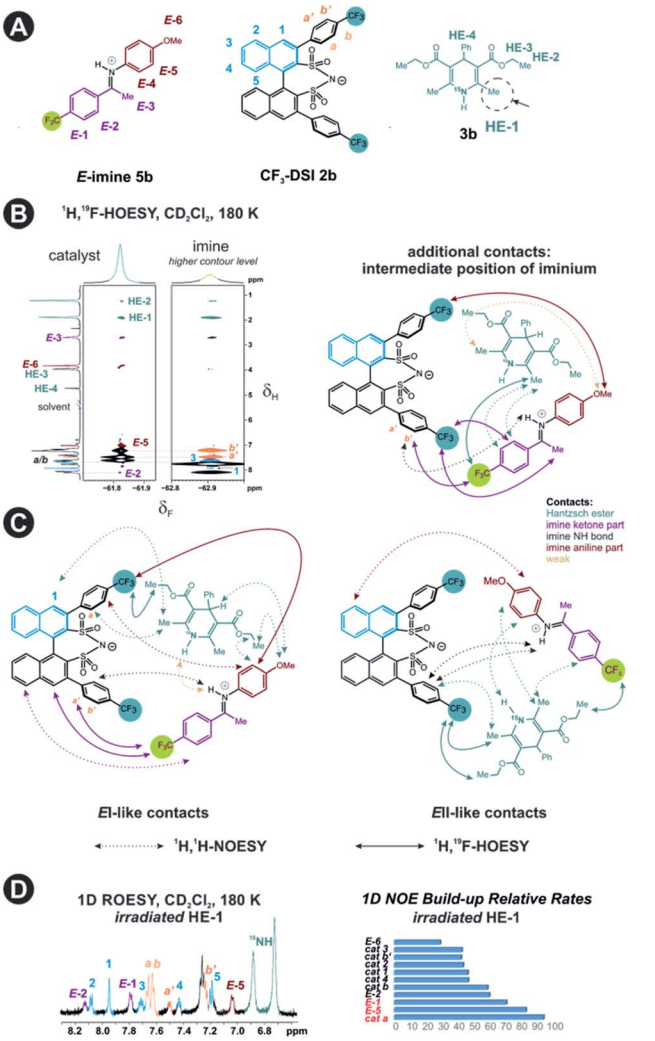

Fig. 3 (A) Structures of *E*-imine **5b**, catalyst **2b** and Hantzsch ester **3b**. (B) 2D ^{1}H,^{19}F-HOESY spectrum showing crosspeaks between the components CF_3-DSI **2b**, Hantzsch ester **3b** (green), imine **5b** (ochre and violet) upon irradiation of HE-1 protons. (C) Schematic structures showing selected intermolecular HOESY (solid line) and NOESY (dotted line) transfers between the catalyst CF_3-DSI **2b**, imine **5b** and Hantzsch ester **3b**. Shown are the contacts typical for two different ternary complex *E*I and *E*II conformers, as well as those suggesting an intermediate position of the imine. (D) 1D ROESY and the relative build-up rates taken from 1D NOESY spectra with different mixing times (25–300 ms) upon the irradiation of HE-1 protons.

species[10] and in calculated transition state structures.[18] The Hantzsch ester would be stacked above or below the imine. The evidence for this conformation comes from the NOE/HOE contacts that could not be assigned to *E*I and *E*II structures (Fig. 3B, right).

With the data in hand, we addressed the orientation of the bound Hantzsch ester in the ternary complex. The NOE/ROEs network detected indicates a bifunctional binding of the Hantzsch ester (*via* a very weak H-bond) and the imine to the catalyst as proposed previously for the CPAs by theoretical calculations and is already shown in Fig. 2B. In the case of the bifunctional binding mode, the Hantzsch ester interacts *via* its

NH group. Indeed, only the neighboring 2,6-dimethyl groups show a significant diastereotopic splitting upon binding in the ternary mixture and show the largest reduction in T_2 relaxation time (further details see ESI Chapter 10†). In addition, these 2,6-dimethyl groups show the strongest intermolecular NOE/ROEs (see ESI Chapter 6.2.3 and 6.2.4†). Thus, the bifunctional binding mode is confirmed and further insight into the position of the Hantzsch ester is exemplified by the relative NOE build-up rates upon selective irradiation of these Hantzsch ester methyl groups (Fig. 3D, right) and a 1D ROESY spectrum (Fig. 3D, left). The close proximity between the two hydrogen bonds in the ternary complex was further confirmed by a selective NOE experiment from the proton of the catalyst/imine hydrogen bond (δ_H 14.53 ppm) to the Hantzsch ester methyl protons and *vice versa*.

For the first time, direct spectroscopic evidence is provided for the bifunctional binding mode of a Brønsted acid catalyst with the substrate and the reagent. In addition, the investigated ternary complexes might show conformational flexibility that reflects the situation in the binary complexes, or a single new conformation with intermediate imine/Hantzsch ester position.

Conformational screening by computational methods

The NMR investigations provided qualitative insight about the contacts within the ternary complex. However, the fast exchange between the binary and the ternary complexes and any potential ternary complex conformational exchange allowed only a qualitative analysis of the NOE patterns discussed above. Therefore, the conformational space of the ternary complex was investigated by computational methods so that the resulting 3D structures could be compared with the experimental data.

Quantitative assessment of binary complexes

Previously, five hydrogen-bonded DSI binary complex conformations have been identified in agreement with the NMR data.[28] These structures correspond to the type E_N, with iminium bound to nitrogen; E_OI, and E_OII-types bound to the oxygen; and *Z*I and *Z*II. Type I structures bring the parent ketone part of the imine closer to the binaphthyl backbone of the catalyst, whereas in type II structures the *N*-aryl substituent is located near the binaphthyl core (for principal contacts see Fig. 3C). Out of these five binary complexes, the previous computational approaches always favoured the E_N-complex while the experiments revealed a significant population of the *Z*-complexes.[28]

This large energetic overestimation of the *E*-imine binary complexes in Brønsted acid catalysis by the applied theoretical methods has been a general problem so far.[10] Since hydrogen bonds and π,π-interactions dominate the interaction mode revealed by NMR, we tested the B97-D functional, as it was developed to adequately describe hydrogen-bonded DNA base pairs.[40,41] Indeed, calculating the Gibbs free energies of the binary complexes by the B97-D/def2-QZVPP/SMD//TPSS-D3(BJ)/def2-SVP/SMD level of theory correctly reproduces for the first time the experimental *E*/*Z* ratio (**2a**/**5a** exp. *E*/*Z* = 88%/12% at 180 K; calc. *E*/*Z* = 87%/13%). Out of the five conformations for $(CF_3)_2$-DSI **2a**/**5a** the major structures are E_N (~87% population), and *Z*II (12%). Furthermore, from 8 tested methods using ORCA computational software,[42] the next best energetic estimation was provided by a more advanced, robust double hybrid B2PLYP/CBS (E_N ~ 93% population, *Z*I ~ 6.5%; see ESI Chapter 14.7†).[43,44] Moreover, the reaction Gibbs free energy of the Hantzsch ester **3d** binding to the binary complex $(CF_3)_2$-DSI **2a**/*Z*-**5a** was best reproduced also by this method (exp. −4.6 kJ mol^{-1}; calc. −9.9 kJ mol^{-1}; see ESI Chapter 14.10†). Thus, an almost quantitative assessment of both relative energies of binary complexes and the binding of the Hantzsch ester could be achieved by selected computational methods.

Ternary complexes

Having established the methods required, we addressed the *E*-ternary complexes because only for those sufficiently detailed structural information was available from the NMR experiments (see above). First, we identified the principal conformers by a conformational search of the ternary complex containing CF_3-DSI **2b**, simplified dimethylester **3c**, and imine *E*-**5b** using GFN2-xTB metadynamics.[45] This search resulted in E_N structures containing an NHN-hydrogen bond to the imine as well as an OHN hydrogen bond to the Hantzsch ester. Additionally, these E_O structures have the iminium bound to a catalyst oxygen. Next, we performed a more extensive search to cover full conformational space – starting from the previous lowest energy structure (E_O) with a more stable conformation of **3c** – and generated 300 conformers (annotated with quotation mark). Then, we optimized the most stable structures with TPSS-D3(BJ)/def2-SVP method (with implicit solvation model) and obtained exclusively conformers containing hydrogen-bonded species (E_N as well as E_O structures for both the imine and the Hantzsch ester). The most energetically favorable candidates from the conformational analyses are the E_NI″ structure and the E''_O structure presented in Fig. 4A (for energetic assessment see discussion below). The structure E_NI″ resembles in principle the relative position of the imine towards the catalyst in the *E*I transition states calculated for CPAs.[18] In addition, the special binding site of the DSI allows for the new conformation E''_O. In the conformation E_NI″ the Hantzsch ester is far away from the imine, making the hydride transfer event unfavourable. In contrast, in the E''_O conformation, both the imine and the Hantzsch ester occupy central positions in close proximity, making this conformation a prospective candidate for the transition state.

However, the E_NI″ conformation cannot accommodate all of the experimental NOE contacts alone in contrast to the conformation E''_O. Its presence at 180 K is corroborated experimentally by all the NOE and HOE contacts. Indeed, this E_O complex is easily accessible at ambient temperature reaction conditions with the reactive form of **3** such as **3a** and is a direct precursor to the *E*-transition state. Detailed structural analysis is given below. To our knowledge, this is the first complex in ion pair catalysis, in which an O–H–N hydrogen bond is preferred over an N–H–N hydrogen bond in presence of a multiple H-bond donor–acceptor system. So far, only for a free IDPi

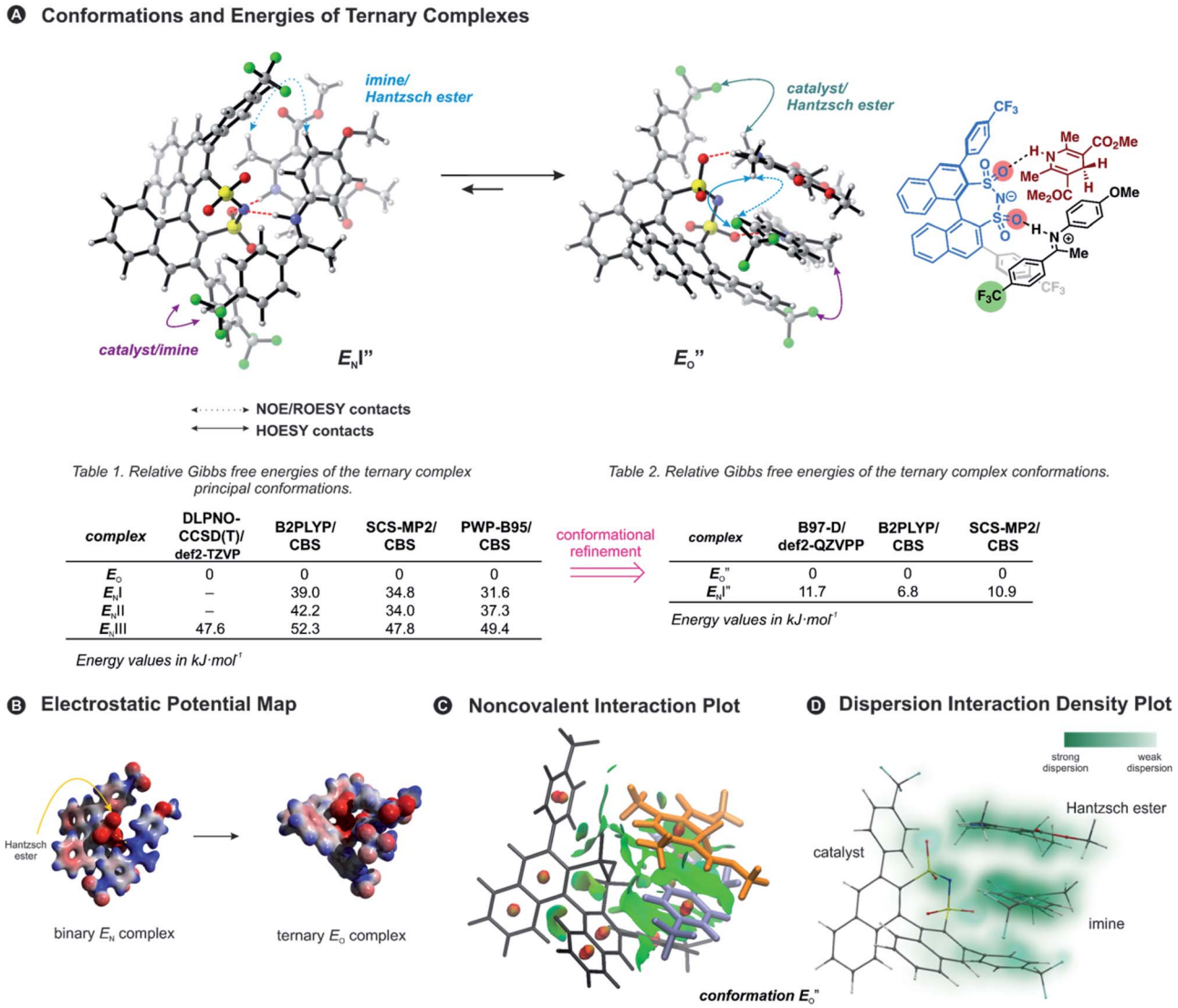

Fig. 4 (A) E''_O and E_NI″ shown here are the computed lowest-energy conformations of the ternary complex CF_3-DSI **2b**/*E*-**5b**/**3c**. E''_O accommodates all the experimental NOE and HOESY connections (key NOEs/HOEs are shown in the structures computed at TPSS-D3(BJ)/def2-SVP/SMD). Table 1 shows $\Delta G_{(DCM,180\ K)}$ for the principal conformations (free energy corrections and solvation corrections at the geometry optimization level of theory were added to the single-point total electronic energies). Table 2 illustrates the relative stabilities $\Delta G_{(DCM,180\ K)}$ of the conformationally refined structures. (B) Binding of the Hantzsch ester occurs at the oxygen atoms as evidenced by electrostatic potential map of the binary E_N and ternary E_O complexes. (C) Noncovalent interaction plot of complex E''_O, suggesting that dispersion contributes significantly to stabilization of the ternary complex. (D) Dispersion interaction density plot confirms the importance of dispersion within complex E''_O (computed at DLPNO-CCSD(T)/def2-TZVP level of theory).

catalyst dimer dynamic structure,[46] and our DSI binary complexes,[28] the possibility of switching between oxygen and nitrogen atoms was proposed.

Next, we calculated the Gibbs free energies of the ternary complexes with different methods for the single-point energy calculation: B97-D and B2PLYP discussed above, one additional double hybrid functional,[47] and SCS-MP2 used previously for CPA complexes in our group (Fig. 4A).[27]

We evaluated the methods based on the experimental data in which substantial populations of some E_N conformers or a substantial population of E''_O are required to potentially detect the distinct NOE contacts and especially the NOE build-up rates discussed above (Fig. 3C and D). However, based on the optimized ternary complex structures and a thorough NOE analysis, it then became clear that the E''_O structure fits all the NOE and HOE data (see ESI Chapter 7.2†). For instance, the **2a**/*E*-**5b**/**3b** complex showed intermolecular HOE contact between methyl group of the imine parent ketone and the 3-substituent of the catalyst, which cannot be found in any of the E_N structures (Fig. 4A).

This E''_O conformation develops considerable dispersion areas between the imine (parent ketone part aromatic ring), the 3,3′-substituent and the Hantzsch ester that compensate for the lack of interactions of the *N*-substituent with the catalyst (for

NCI plot see Fig. 4C and ESI Chapter 14.8.7†). This may explain high enantioselectivities of *N*-methyl and *N*-unsubstituted imines. Therefore, appropriate computational methods should reflect a high population of the E''_O complex.

All the computational methods predict E''_O as the most stable conformation for the solution-phase geometry-optimized structures from both conformational searches (see Fig. 4A). In addition, after the principal conformational search, we conducted a DLPNO-CCSD(T) calculation that confirms the energetic bias between the principal E_O and a similar E_N conformation towards the E_O structure. This was in agreement with the other computational methods used in the principal conformational search (see ESI 14.8†).[48,49] Local energy decomposition at DLPNO-CCSD(T)/def2-TZVP level of theory shows the dispersion, electrostatics and exchange contribution in two complexes compared to binary E_N complex (see ESI 14.9.1†).[50–52] A stabilizing dispersion interaction develops between the imine and the Hantzsch ester in the ternary complex.

Moreover, the binding energy was decomposed, confirming larger binding energy of the E_O complex. The energy decomposition showed that the electron preparation (destabilization by geometrical strain) is compensated by the gain in electrostatic energy (presumably including the hydrogen bond), and the extra stabilization which is provided by dispersion and exchange energy can aid in the ternary complex formation. Indeed, for the E_O conformation, the electron preparation penalty is lower than in the E_N complex and less geometrical distortion is thus required in the binding process. The dispersion interaction density plot of the E''_O complex shows the interaction between the CF_3-DSI catalyst **2b** and imine **5b**, where the strongest dispersion is at the catalyst O and N atoms constituting the hydrogen bond (Fig. 4D). Dispersion is thus vital in stabilization of the pre-reacting complexes.

In line with the energy decomposition, the electrostatic potential surface map of CF_3-DSI **2b**/imine **5b**/Hantzsch ester **3c** revealed the potential binding sites as the sites providing electrostatic or hydrogen-bond interactions with the Hantzsch ester. This map shows significant negative charge located at the nitrogen and oxygens of the DSI catalyst in its E_N binary complex (Fig. 4B), attracting the Hantzsch ester to develop a hydrogen bond resulting in the bifunctional activation. The negative charge is slightly reduced upon the binding of the Hantzsch ester to form the ternary complex.

The energetic preference of conformation E''_O, which matches the NMR data, is given by the B2PLYP method and is in line with the binary complex energetics and *Z*-binding equilibrium calculations. Therefore, this method seems to be universal to describe the energetics in this study, in contrast to other methods which over- or underestimate some of the species.

Overall, for the first time the ratio of *E*- and *Z*-imine binary complexes were correctly reproduced by computational methods. The calculations for the DSI *E*-ternary complexes revealed the major conformation E''_O and disfavored E_NI'' conformation. The E''_O conformation has an intermediate position of both the imine and the Hantzsch ester; and resembles a precursor for the transition state. In addition, E''_O provides exclusively dispersion areas to the 3,3′-substituents and the Hantzsch ester, which may explain the high enantioselectivities for *N*-Me imines and NH imine hydrochloride salts.[36]

DFT computations of NMR spectra

The binary complexes of the DSIs and imines are in fast exchange with the ternary complex. Therefore, we computed NMR data to distinguish between the binary and ternary complex contributions. To calibrate the computed NMR parameters (δ_H, δ_N) on direct experimental data, first a set of DSI *E*- and *Z*-imine binary complexes as well as free imines and Hantzsch ester were selected as model systems. We plotted the computed chemical shifts at the TPSS/pcSseg-3/SMD level of theory against the experimental chemical shifts to derive a linear scaling factor.[53] Then, this computed NMR scaling was applied to the calculated NMR parameters (δ_H, δ_N) of ternary structures (see ESI Chapters 14.11–14.13 for details†). Indeed, these conformations do not show significantly different chemical shifts. Thus, calculations corroborate the small chemical shift difference for the *E*-complexes upon binding of the Hantzsch ester.

From ternary complexes to transition states

Two transition state structures, **TS-*E*-*R*** and **TS-*Z*-*S*** (+40.1 kJ mol^{-1}), were found based on the most stable *E*- and *Z*-ternary complexes. Interestingly, all the transition state complexes are *O*,*O*-bonded transition structures (Fig. 5A and C). The structures of **TS-*E*-*R*** and **TS-*Z*-*S*** and their noncovalent interactions (NCI) plots are given in Fig. 5A.[54,55] There is no notable dispersion area in the **TS-*Z*-*S*** structure, similar to the situation in the ternary *Z*-complex. In contrast, the **TS-*E*-*R*** reveals a very prominent interaction area – a triple-stacked π–π-complex – where imine is stacked between a catalyst 3,3′-substituent and Hantzsch ester (see ESI Chapter 14.8.7†). These attractive interactions compensate for the steric repulsion which is prominent in the non-compact *E*-ternary complexes and transition states. Both interactions seem to be negligible in the more compact *Z*-complexes which explains the comparable energies of *E*- and *Z*-complexes. The relative energetics of the transition states are in accordance with the major product, the (*R*)-enantiomer. However, the high energetic difference would predict its exclusive formation, which is in contrast with the experimentally observed enantioselectivity (er 69 : 31). Recently, an exceptional example was reported of the conformational search and energetics' evaluation of hundreds of transition structures in ion-pair catalysis.[52] However, in our investigated transfer-hydrogenation reaction the high activation barriers prohibit the reverse reactions or equilibration.

This means the transfer hydrogenation is under kinetic control and the reaction barriers from the intermediate complexes to the transition states determine the stereoselectivity.[56] Moreover, additional photoisomerization/back-isomerization experiments show that the thermal *E*/*Z*-isomerization barrier within the binary complex is higher than the hydride step at 298 K (see Fig. 5B and ESI Chapter 12†). As

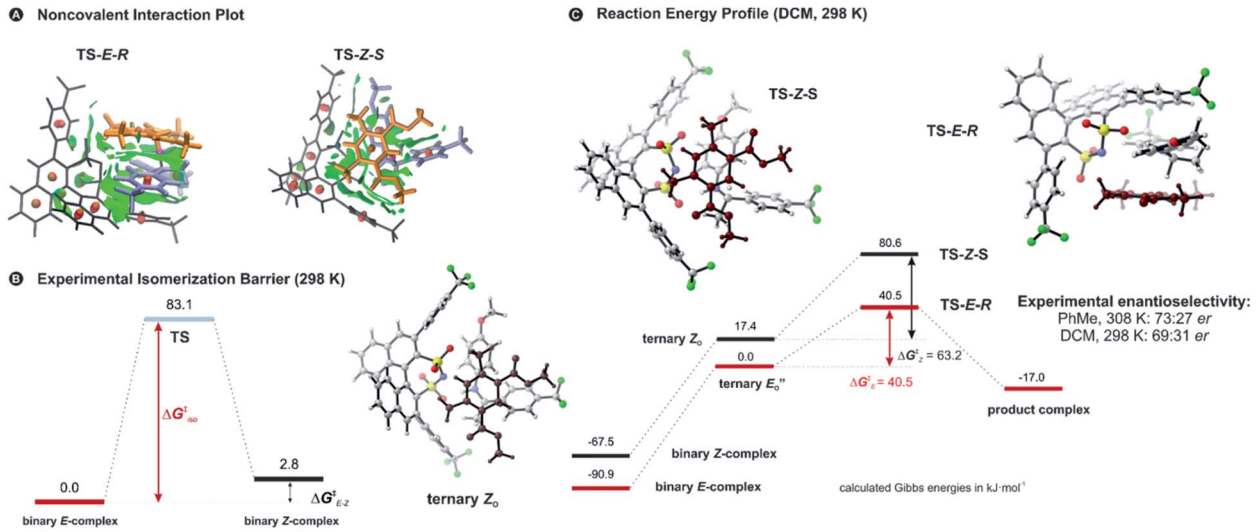

Fig. 5 (A) Noncovalent interaction plot (NCI) of TS-*E*-*R* and TS-*Z*-*S* showing large stabilizing interaction areas in the TS-*E*-*R* structure, which are reduced in the more compact *Z*-structure. Hantzsch ester **3c** is shown in orange and imine **5b** in blue colour. (B) The high experimental isomerization barrier of binary complex CF_3-DSI **2b** and imine **5b** shows that the isomerization is potentially the rate-determining step. (C) Reaction energy profile with Gibbs energies at 298 K (computed at B2PLYP-D3(BJ)/CBS//TPSS-D3(BJ)/def2-SVP/(gas phase, 298 K) with SMD solvation correction), showing smaller energetic barrier for the ternary E''_O complex. The inclusion of late intermediates (ternary complexes) in the profile shifts the $\Delta\Delta G^{\ddagger}$ closer to the experimental value. Hantzsch ester is shown in dark brown colour.

a result, this very slow isomerization of the binary complexes cannot be regarded as a fast *E*/*Z* pre-equilibrium. Thus, the classic Curtin–Hammett principle cannot be applied,[57] as "the product composition is formally related to relative concentrations of the conformation isomers".[58]

Therefore, for the $\Delta G^{\ddagger}$ values, not only individual transition states energies but also the stabilities of the intermediates have to be considered. In addition, in this study multiple experimental data are available about the ground states and the energetics of late intermediates.

The calculated reaction energy profile (Fig. 5C) allows for the energetic barrier assessment from E''_O to **TS-*E*-*R*** ($\Delta G^{\ddagger}_{DCM,298}$ 40.5 kJ mol^{-1}). Compared to that, the energetic barrier from the lowest energy Z_O-ternary complex to the transition state **TS-*Z*-*S*** is higher in energy ($\Delta G^{\ddagger}_{DCM,298}$ 63.2 kJ mol^{-1}). While this energetic offset still suggests the exclusive formation of the major *R*-enantiomer (experimental er 69 : 31 *R* : *S*), the inclusion of the intermediate energetics shifts the theoretical values towards the correct experimental enantioselectivity.

Within this combined analysis of experimental and computational data, each step of computational level was backed by experimental data and used for the selection of the theoretical method. Overall, this approach shows the importance of ground states and their energetics when investigating stereoselectivity in kinetically controlled reactions without fast pre-equilibration of the intermediates.

Conclusions

In summary, we present detailed experimental data about 6 *E*- and *Z*-ternary complexes between DSI catalysts, imines and a Hantzsch ester. This is to our knowledge the first detailed experimental data of ternary complexes in ion pairing catalysis at all. Extensive intermolecular NOE and HOE contacts at low temperatures, chemical shift mapping, diffusion and relaxation data were used as the experimental basis for the structure elucidation. In this study, experiments and calculations together indicate the unexpected energetic preference of the iminium binding to an oxygen in the presence of a nitrogen as an H-bond acceptor. This is reflected in the higher population of the ternary complex E''_O compared to the E_N-complexes which is typical for the binary complexes. Furthermore, this is to our knowledge the first detailed spectroscopic proof for a bifunctional binding mode proposed earlier for CPAs by theoretical work and thermodynamic arguments.

Moreover, this study convincingly demonstrates that the combination of experimental and computational analyses of late intermediates in ion pair catalysis is necessary for the interpretation of transition states. The correct energetic assessment of ion pairs is most critical in computational chemistry, so in this study, the complexes and binding events were used as key to select computational tools and to validate the essential calculations. This approach allowed us for the first time to reproduce correct populations of the binary complexes. Furthermore, the consideration of the reaction barriers from the ternary complexes to TSs showed the importance of structures and energetics of late intermediates in case of high isomerization barriers.

Overall, this study shows that ternary complex formation is favoured for catalysts with an open binding site and that in case of multiple hydrogen-bond donors the hydrogen bond can switch between the binary and ternary complexes leading to more favourable conformers resembling the transition states. The rather weak binding of the second substrate and the

preferential stabilization of the transitions states by hydrogen bonding resembles enzymatic catalysis. In contrast to the CPAs, in which the strong hydrogen bond, rigid complexes and specific noncovalent interactions govern the stereoselectivity, the DSIs can adopt a more favourable conformation by hydrogen bond switching in the ternary complexes. For DSIs a strong and rigid hydrogen bond as adopted in CPAs would be detrimental to the stereoselectivity. In the dynamic system of the DSIs the substrate position in the TS provides mainly interactions of the parent ketone part of the imine with catalyst 3,3′-substituent. This explains the enhancement in enantioselectivity for *N*-methyl imines with no additional stabilization from the *N*-substituent. On the other hand, decrease in enantioselectivity with the electronic variation of the aryl imines corroborates a demand for a weak hydrogen bond. Thus, DSIs have the potential to combine high flexibility and high stereoselectivity, which offers an advantage over enzymatic catalysis, where more flexible and promiscuous enzymes are also less selective.[59] It may also confirm the concept of structural flexibility as a vital point in asymmetric catalysis.[60]

Author contributions

M. Ž. and R. M. G. conceived and conceptualised the project. M. Ž. performed the experiments, DFT calculations, and visualisations. R. M. G. supervised the project and acquired funding. Both authors analysed the data, prepared and revised the manuscript.

Conflicts of interest

There are no conflicts to declare.

Acknowledgements

Financial and intellectual support was provided by the European Research Council (ERC-CoG 614182 – IonPairsAtCatalysis) and the DFG (SPP 1807 Control of London Dispersion Interactions in Molecular Chemistry). Additional intellectual support from DFG (RTG 2620 Ion Pair Effects in Molecular Reactivity) is acknowledged.

Notes and references

1 P. Renzi, J. Hioe and R. M. Gschwind, *Acc. Chem. Res.*, 2017, **50**, 2936–2948.
2 M. Žabka and R. Šebesta, *Molecules*, 2015, **20**, 15500–15524.
3 D. Parmar, E. Sugiono, S. Raja and M. Rueping, *Chem. Rev.*, 2014, **114**, 9047–9153.
4 M. Terada, *Synthesis*, 2010, 1929–1982.
5 M. Rueping, A. Kuenkel and I. Atodiresei, *Chem. Soc. Rev.*, 2011, **40**, 4539–4549.
6 M. Rueping, E. Sugiono, C. Azap, T. Theissmann and M. Bolte, *Org. Lett.*, 2005, **7**, 3781–3783.
7 R. I. Storer, D. E. Carrera, Y. Ni and D. W. C. Macmillan, *J. Am. Chem. Soc.*, 2006, **128**, 84–86.
8 A. M. Faísca Phillips and A. J. L. Pombeiro, *Org. Biomol. Chem.*, 2017, **15**, 2307–2340.
9 N. Sorgenfrei, J. Hioe, J. Greindl, K. Rothermel, F. Morana, N. Lokesh and R. M. Gschwind, *J. Am. Chem. Soc.*, 2016, **138**, 16345–16354.
10 M. Melikian, J. Gramüller, J. Hioe, J. Greindl and R. M. Gschwind, *Chem. Sci.*, 2019, **10**, 5226–5234.
11 N. Lokesh, J. Hioe, J. Gramüller and R. M. Gschwind, *J. Am. Chem. Soc.*, 2019, **141**, 16398–16407.
12 L. Simón and J. M. Goodman, *J. Am. Chem. Soc.*, 2008, **130**, 8741–8747.
13 L. Simón and J. M. Goodman, *J. Org. Chem.*, 2011, **76**, 1775–1788.
14 J. P. Reid and J. M. Goodman, *J. Am. Chem. Soc.*, 2016, **138**, 7910–7917.
15 J. P. Reid and J. M. Goodman, *Chem.–Eur. J.*, 2017, **23**, 14248–14260.
16 R. Maji, S. C. Mallojjala and S. E. Wheeler, *Chem. Soc. Rev.*, 2018, **47**, 1142–1158.
17 T. Marcelli, P. Hammar and F. Himo, *Chem.–Eur. J.*, 2008, **14**, 8562–8571.
18 P. Renzi, J. Hioe and R. M. Gschwind, *J. Am. Chem. Soc.*, 2017, **139**, 6752–6760.
19 L. Simón and J. M. Goodman, *J. Am. Chem. Soc.*, 2009, **131**, 4070–4077.
20 P. García-García, F. Lay, P. García-García, C. Rabalakos and B. List, *Angew. Chem., Int. Ed.*, 2009, **48**, 4363–4366.
21 T. James, M. Van Gemmeren and B. List, *Chem. Rev.*, 2015, **115**, 9388–9409.
22 V. N. Wakchaure, P. S. J. Kaib, M. Leutzsch and B. List, *Angew. Chem., Int. Ed.*, 2015, **54**, 11852–11856.
23 M. Hatano and K. Ishihara, *Asian J. Org. Chem.*, 2014, **3**, 352–365.
24 T. Akiyama and K. Mori, *Chem. Rev.*, 2015, **115**, 9277–9306.
25 M. Benda and S. France, *Org. Biomol. Chem.*, 2020, **18**, 7485–7513.
26 V. N. Wakchaure and B. List, *Angew. Chem., Int. Ed.*, 2016, **55**, 15775–15778.
27 J. Greindl, J. Hioe, N. Sorgenfrei, F. Morana and R. M. Gschwind, *J. Am. Chem. Soc.*, 2016, **138**, 15965–15971.
28 K. Rothermel, M. Žabka, J. Hioe and R. M. Gschwind, *J. Org. Chem.*, 2019, **84**, 13221–13231.
29 A. Galván, A. B. González-Pérez, R. Álvarez, A. R. de Lera, F. J. Fañanás and F. Rodríguez, *Angew. Chem., Int. Ed.*, 2016, **55**, 3428–3432.
30 C. Zheng and S. L. You, *Chem. Soc. Rev.*, 2012, **41**, 2498–2518.
31 G.-B. Shen, Y.-H. Fu and X.-Q. Zhu, *J. Org. Chem.*, 2020, **85**, 12535–12543.
32 M. Rueping, J. Dufour and F. R. Schoepke, *Green Chem.*, 2011, **13**, 1084–1105.
33 J. D. Yang, J. Xue and J. P. Cheng, *Chem. Soc. Rev.*, 2019, **48**, 2913–2926.
34 J. F. Schneider, M. B. Lauber, V. Muhr, D. Kratzer and J. Paradies, *Org. Biomol. Chem.*, 2011, **9**, 4323–4327.
35 K. Rothermel, M. Melikian, J. Hioe, J. Greindl, J. Gramüller, M. Žabka, N. Sorgenfrei, T. Hausler, F. Morana and R. M. Gschwind, *Chem. Sci.*, 2019, **10**, 10025–10034.

36 V. N. Wakchaure, C. Obradors and B. List, *Synlett*, 2020, 1707–1712.
37 W. Tang, S. Johnston, J. A. Iggo, N. G. Berry, M. Phelan, L. Lian, J. Bacsa and J. Xiao, *Angew. Chem., Int. Ed.*, 2013, **52**, 1668–1672.
38 M. P. Williamson, in *Encyclopedia of Analytical Science*, ed. P. Worsfold, C. Poole, A. Townshend and M. Miró, Elsevier, Amsterdam, 3rd edn, 2019, pp. 264–271.
39 T. D. W. Claridge, *High-Resolution NMR Techniques in Organic Chemistry*, Elsevier, Boston, 3rd edn, 2016, pp. 315–380.
40 J. Antony and S. Grimme, *Phys. Chem. Chem. Phys.*, 2006, **8**, 5287–5293.
41 S. Grimme, *J. Comput. Chem.*, 2006, **27**, 1787–1799.
42 F. Neese, *Wiley Interdiscip. Rev.: Comput. Mol. Sci.*, 2018, **8**, 4–9.
43 S. Grimme, *J. Chem. Phys.*, 2006, **124**, 34108.
44 B. Schirmer and S. Grimme, in *Frustrated Lewis Pairs I*, ed. G. Erker and D. W. Stephan, Springer, Heidelberg, 2013, pp. 213–230.
45 S. Grimme, *J. Chem. Theory Comput.*, 2019, **15**, 2847–2862.
46 H. Kim, G. Gerosa, J. Aronow, P. Kasaplar, J. Ouyang, J. B. Lingnau, P. Guerry, C. Farès and B. List, *Nat. Commun.*, 2019, **10**, 1–6.
47 L. Goerigk and S. Grimme, *J. Chem. Theory Comput.*, 2011, **7**, 291–309.
48 C. Riplinger, B. Sandhoefer, A. Hansen and F. Neese, *J. Chem. Phys.*, 2013, **139**, 134101.
49 M. Sparta and F. Neese, *Chem. Soc. Rev.*, 2014, **43**, 5032–5041.
50 W. B. Schneider, G. Bistoni, M. Sparta, M. Saitow, C. Riplinger, A. A. Auer and F. Neese, *J. Chem. Theory Comput.*, 2016, **12**, 4778–4792.
51 G. Bistoni, *Wiley Interdiscip. Rev.: Comput. Mol. Sci.*, 2020, **10**, e1442.
52 D. Yepes, F. Neese, B. List and G. Bistoni, *J. Am. Chem. Soc.*, 2020, **142**, 3613–3625.
53 M. W. Lodewyk, M. R. Siebert and D. J. Tantillo, *Chem. Rev.*, 2012, **112**, 1839–1862.
54 E. R. Johnson, S. Keinan, P. Mori-Sánchez, J. Contreras-García, A. J. Cohen and W. Yang, *J. Am. Chem. Soc.*, 2010, **132**, 6498–6506.
55 R. Laplaza, F. Peccati, R. A. Boto, C. Quan, A. Carbone, J. P. Piquemal, Y. Maday and J. Contreras-García, *Wiley Interdiscip. Rev.: Comput. Mol. Sci.*, 2020, 1–18.
56 Q. Peng, F. Duarte and R. S. Paton, *Chem. Soc. Rev.*, 2016, **45**, 6093–6107.
57 J. Burés, A. Armstrong and D. G. Blackmond, *J. Am. Chem. Soc.*, 2012, **134**, 6741–6750.
58 P. Muller, *Pure Appl. Chem.*, 1994, **66**, 1077–1184.
59 A. J. T. Smith, R. Müller, M. D. Toscano, P. Kast, H. W. Hellinga, D. Hilvert and K. N. Houk, *J. Am. Chem. Soc.*, 2008, **130**, 15361–15373.
60 J. M. Crawford and M. S. Sigman, *Synthesis*, 2019, **51**, 1021–1036.